

# The coalescence of combustion-sprayed ethylene–methacrylic acid copolymer

J. A. BROGAN\*, C. C. BERNDT

*Department of Materials Science and Engineering, State University of New York at Stony Brook, Stony Brook, NY 11794, USA*

A design of experiments approach was employed to study the coalescence of combustion-sprayed ethylene–methacrylic acid copolymer (EMAA). The powder feed rate, stand-off distance, substrate temperature, propane flow rate, and compressed air flow rate were studied by using a  $2^{5-1}$  factorial design matrix. Empirical models were developed to predict coating surface roughness, coating temperature and splat elongation ratio. Such methods allow process optimization, estimation of interactions among parameters, and the determination of the factors which influence the coalescence of ethylene–methacrylic acid copolymer coatings.

## 1. Introduction

Thermal spraying of polymers is gaining increased attention because the ability to apply relatively thin (75  $\mu\text{m}$ ) and thick (5 mm) coatings of polymers on to a wide variety of materials is an effective method to produce protective barrier coatings. Protection of the infrastructure from the effects of corrosion is a growing concern [1–4]. The once, highly accepted lead-based alkyd paints have an extended history of satisfactory performance, but can no longer be used due to the health risks associated with lead exposure. The most recent amendment to the 1990 Clean Air Act allows restrictions to be placed on paints and solvents containing volatile organic compounds (VOCs). Most industrial paints are now limited to a maximum VOC content of 350  $\text{g l}^{-1}$ . Thermal spraying is one viable option to the coatings industry because it is a 100% solids process with minimal VOCs. Thermoplastic spraying, therefore, provides an environmentally sensitive alternative to paint and other organic formulations.

Thermally sprayed polymer coatings are generally manufactured by the melting of polymer powder in a combustion flame [5]; however, a plasma or high-velocity fuel gases may also be used [6, 7]. Powder is axially fed into the combustion zone via compressed air. The polymer particulates are propelled through the flame where, upon melting, they are transported to the pre-heated substrate. As the molten particles impinge on the substrate, the well-heated particles will deform and solidify, forming an interlaced network of splats. The thickness of the coating is governed by the number of repeated passes of the spray gun across the substrate as well as the powder feed rate. Polymer powders are specified by their chemistry, morphology, molecular weight distribution or melt-flow index, and particle-size distribution. Spray parameters must be

selected to accommodate each particular polymer formulation. Polymeric materials that have been sprayed include polyethylene, polypropylene, polyamide, polytetrafluoroethylene copolymer, ethylene–methacrylic acid copolymer, and post-consumer commingled polymer.

Polymer spraying is a one-coat process which acts as both the primer and the sealer, with no additional cure times, unlike the traditional three-coat painting processes [8]. Thermoplastic coatings can be repaired by re-melting and applying additional material to the desired location. In addition, polymers such as ethylene–methacrylic acid copolymer (EMAA) can be applied in high humidity conditions as well as at temperatures below freezing [9, 10]. Applications of polymer coatings include structural steel coatings, external pipe coatings, transfer chutes, chemical containment and light poles where high chemical resistance and high impact resistance are used to advantage.

The processing factors responsible for changes in the microstructure of thermally sprayed polymer coatings are not well-documented. A design of experiments (DOE) approach was employed to eliminate the current "trial and error" methods. In this fashion, knowledge and understanding of how process parameters affect the melting and fusion of EMAA copolymer will not only serve as an optimization procedure for EMAA, but will provide insight in to the application of other macromolecules.

## 2. Experimental procedure

### 2.1. Spray torch

A combustion torch marketed by Plastic FlameCoat Systems (Big Spring, TX) as PF200 was used with the addition of a fluidized-bed powder delivery system [11]. This torch used propane at 41 kPa and

\*Author to whom all correspondence should be addressed

compressed air at 827 kPa as the fuel and oxidant for the combustion process. Flow rates of either gas can be varied to (i) lengthen the flame by increasing the propane flow rate, or (ii) to alter the oxidizing/reducing character of the flame by altering the air flow rate. The maximum flame temperature is approximately 2000 °C [12].

## 2.2. Materials

The ethylene–methacrylic acid copolymer was obtained from Plastic FlameCoat Systems as PF113W, Fig. 1. This particular grade of EMAA has a melt index of 500 g/10 min, corresponding to the lowest average molecular weight copolymer in the EMAA series. The average particle size was 155 μm as measured by Microtrac™ particle-size analysis. A standard deviation of 82 μm indicates that the powder has a large particle-size distribution.

Cold-rolled steel sheet was wiped with propanol to remove grease and subsequently grit-blasted at 80 p.s.i. (10<sup>3</sup> p.s.i. = 6.89 N mm<sup>-2</sup>) with alumina grit. The surface roughness of the prepared steel sheet measured 8–10 μm using a mechanical stylus profilometer (Mitutoyo, model SurfTest III).

## 2.3. Design of experiments

A 2<sup>5-1</sup> factorial design matrix was chosen for EMAA copolymer to determine the processing factors responsible for changes in the coating microstructure. Using a two-level design, process parameters were varied from a low value (–) to a high value (+) and the effect upon a particular response, Y, was measured. The "effect" was calculated by subtracting the average response using the low parameter from the

average response using the high parameter setting [13] i.e.

$$Effect = \frac{\sum Y_+}{n_+} - \frac{\sum Y_-}{n_-} \quad (1)$$

Interactions between parameters can also be detected and quantified [13]. Influential process parameters can, therefore, be identified on the basis of the induced effect. The underlying objective of empirical modelling was to relate N coded process parameters  $X_i$  ( $i = 1 \dots N$ ; here  $N = 5$ ) to M responses  $Y_j$  ( $j = 1 \dots M$ ; here  $M = 3$ ) of the form

$$Y_j = \beta_0 + \beta_1 X_1 + \beta_2 X_2 + \beta_{12} X_1 X_2 + \beta_3 X_3 + \beta_{13} X_1 X_3 + \beta_{23} X_2 X_3 \dots \beta_{iN} X_i X_N \quad (2)$$

where the beta coefficients are regression coefficients calculated from the measured effect [13] i.e.

$$\beta = \frac{Effect}{2} \quad (3)$$

The  $X_i$  terms in the polynomial equation are coded process parameters representing the selected parameter value multiplied by an empirical factor calculated from the chosen high and low values (+ and –, respectively).

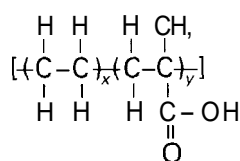
$$X_{coded} = \frac{X - [(+) + (-)]}{[(+) - (-)]} \quad (4)$$

This allows prediction of a particular response on the basis of the selected process parameters.

The present model entails setting five parameters (powder feed rate, stand-off distance, substrate pre-heat temperature, propane flow rate, and compressed air flow rate), at two levels (+ and –), measuring three responses (surface roughness, coating temperature and splat elongation ratio), and calculating the effects due to each parameter and parameter interaction. A design of experiments software package entitled Design-Ease (Statease Inc., Minneapolis, MN) was used to generate the half-factorial matrix, calculate the single parameter and interaction effects, and provide the analysis of variance (ANOVA). Three additional sets of parameters using mean high/low values were also used to account for non-linearity as well as to determine the repeatability of the deposition process, giving a total of 19 experiments. A number of fixed and variable parameters were selected on the basis of thermal spray experience (Table I). A six-axis articulated robot was used to ensure that the traverse speed, stand-off distance and spray-step distance remained constant during spraying.

## 2.4. Characterization

Upon completion of each experiment in the matrix, a remote infrared pyrometer measured the surface temperature of the sprayed deposit, noted as response 1. The surface roughness,  $R_a$ , was assessed using a profilometer which measured the average deviation of the surface from a centreline value, noted as response 2. Settings were chosen to ensure that the stylus recorded



(a)

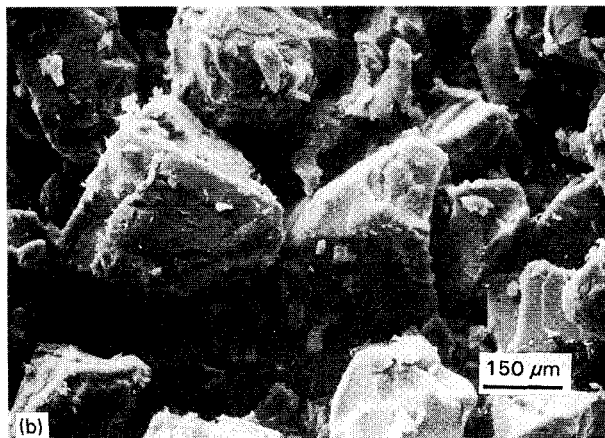


Figure 1 (a) EMAA powder chemistry and (b) morphology

TABLE I Combustion spray parameters

Fixed parameters	Variable parameters
Propane tank pressure 41 kPa	Powder feed rate 70 and 140 gm i n <sup>-1</sup>
Nitrogen tank pressure 345 kPa	Stand-off distance 25 and 50 cm
Compressed air pressure 827 kPa	Substrate preheat temp 21 and 87 °C
Robotic tracerse speed 25 cm s <sup>-1</sup>	Propane flow rate 6.6 and 15.1 L min <sup>-1</sup>
Spray step distance 3 cm	Compressed air rate 120 and 200 L min <sup>-1</sup>

the roughness of the surface undulations rather than the roughness within the undulation. Specimens were cut with a diamond saw, mounted in cross-section and polished using a Buehler Ecomet 3 automated polishing machine (Lake Bluff, IL). Light microscopy, operated in the dark-field imaging condition, allowed imaging of the polymer lamellae. The Buehler image analysis software was used to trace the region of interest which was then digitized for subsequent measurements. Thirty splats per sample were analysed to determine the average elongation ratio of the splat, noted as response 3.

Particle velocities were measured using a Laser-Strobe™ Control Vision System (Idaho Falls, ID) [14]. This system uses two nitrogen laser strobes (5 ns pulse width) with fibre optic cable, to transport and focus 337 nm light to the area of interest. The high-speed electronic shutter (50 ns to 5 µs) was synchronized with the laser flashes. The laser was also synchronized with the framing of the video sensor (5 ns at 337 nm) and was fired once for each captured video frame. The moving particle was effectively frozen in space and displaced in flight (under double-exposure

conditions). The velocity of the particle was calculated from the laser synchronization time and particle displacement.

### 3. Results

The components of the 2<sup>5-1</sup> factorial matrix, as well as the measured responses for each set of experimental conditions, are listed in Table II. The effects of the five uncoded parameters and the interaction effects between the uncoded parameters were calculated for each measured response. Regression coefficients were calculated for each statistically significant effect. Table III summarizes the parameters and/or parameter combinations inducing the greatest effects on the responses. A description of the most important effects will be given for each response and the effects of lesser importance will be stated if used in the model.

#### 3.1. Coating temperature

The temperature of the deposited thermoplastic coating depends upon the substrate preheat temperature

TABLE II 2<sup>5-1</sup> design for EMAA copolymer<sup>a</sup>

Specimen number	Powder feed rate	Stand-off distance	Substrate preheat temp.	Propane flow rate	Air flow rate	Response 1	Response 2	Response 3
	$X_1$ (g min <sup>-1</sup> )	$X_2$ (cm)	$X_3$ (°C)	$X_4$ (L min <sup>-1</sup> )	$X_5$ (L min <sup>-1</sup> )	$Y_{\text{temperature}}$ Deposit temperature (°C)	$Y_{\text{roughness}}$ Surface roughness (µm)	$Y_{\text{ER}}$ Splat elongation ratio
1	70	25	21	6.6	200	60	40	2.06
2	140	25	21	6.6	120	74	22	2.85
3	70	50	21	6.6	120	69	28	4.81
4	140	50	21	6.6	200	96	10	5.13
5	70	25	87	6.6	120	118	20	4.02
6	140	25	87	6.6	200	151	12	4.33
7	70	50	87	6.6	200	121	50	1.59
8	140	50	87	6.6	120	157	10	5.49
9	70	25	21	15.1	120	78	43	2.33
10	140	25	21	15.1	200	108	16	3.85
11	70	50	21	15.1	200	77	48	2.20
12	140	50	21	15.1	120	119	8	5.40
13	70	25	87	15.1	200	160	11	4.21
14	140	25	87	15.1	120	151	11	3.53
15	70	50	87	15.1	120	171	11	4.73
16	140	50	87	15.1	200	182	3	7.33
17	125	38	54	10.9	160	129	13	5.03
18	125	38	54	10.9	160	138	11	4.98
19	125	38	54	10.9	160	131	9	5.98

<sup>a</sup> The  $X_1$  to  $X_5$  and  $Y_{\text{temperature}}$ ,  $Y_{\text{roughness}}$  and  $Y_{\text{ER}}$  refer to the variables and responses used in the empirical modelling within the text.

TABLE III Statistically significant parameters<sup>a</sup>

Deposit temperature (°C)	Surface roughness. $R_a$ (μm)	Splat elongation ratio
Substrate temperature Effect = 66	Powder feed rate Effect = 20	Powder feed rate Effect = 1.5
Propane flow rate Effect = 25	Substrate temperature Effect = 11	Stand-off distance Effect = 1.2
Powder feed rate Effect = 23	Substrate temperature propane flow rate Effect = 9	Powder feed rate compressed air rate Effect = 1.2
	Powder feed rate stand-off distance Effect = 7	Powder feed rate stand-off distance Effect = 1.0
		Substrate temperature Effect = 0.83

<sup>a</sup> The process parameters are presented in descending order of influence.

$X_3$ , the propane flow rate  $X_4$ , and the powder feed rate  $X_5$ . Stand-off distance  $X_2$ , and the interaction between stand-off distance with compressed air,  $X_{12}$ , are also included in the model due to minor contributions. An increase of substrate temperature from ambient to 87 °C increased the coating temperature from 85 °C to 151 °C (effect = 66 °C) when averaged over all parameter combinations in the matrix. Increasing the propane flow rate from its low flow setting to the high flow setting increased the coating temperature from 106 °C to 131 °C (effect = 25 °C). Because the length of the flame increases with the propane rate, higher particle temperatures result from greater residence times within the flame. The average coating temperature increased from 107 °C to 130 °C (effect = 23 °C) when the powder injection rate increased from 70 g min<sup>-1</sup> to 140 g min<sup>-1</sup>. The polynomial equation which empirically predicts the coating temperature (°C) to within 5% is

$$Y_{\text{temperature}} = 118.3 + 11.5X_{1\text{ coded}} + 5.8X_{2\text{ coded}} + 33.1X_{3\text{ coded}} + 12.5X_{4\text{ coded}} - 6.1X_{2\text{ coded}}X_{5\text{ coded}} \quad (5)$$

where the coded  $X_i$  terms are shown below and are applicable to each of the empirical equations representing coating temperature, surface roughness, and splat elongation ratio

$$X_{1\text{ coded}} = \frac{X_1 - 105}{35} (\text{g min}^{-1}) \quad (6)$$

$$X_{2\text{ coded}} = \frac{X_2 - 37.5}{12.5} (\text{cm}) \quad (7)$$

$$X_{3\text{ coded}} = \frac{X_3 - 54}{33} (^\circ\text{C}) \quad (8)$$

$$X_{4\text{ coded}} = \frac{X_4 - 10.9}{4.3} (\text{L min}^{-1}) \quad (9)$$

$$X_{5\text{ coded}} = \frac{X_5 - 160}{40} (\text{L min}^{-1}) \quad (10)$$

The accuracy of Equation 5 was assessed by using the process parameters from the DOE study. Table II, and comparing the measured response to the predicted response. The 5% error represents the average residual from the experimental matrix.

### 3.2. Surface roughness

The roughness of EMAA coatings depends upon the powder feed rate  $X_1$ , substrate temperature  $X_3$ , substrate temperature/propane flow rate interaction,  $X_{34}$  and powder feed rate/stand-off distance interaction,  $X_{12}$ . The propane flow rate,  $X_4$ , was also included in the model for increased accuracy. An  $\ln(Y_2)$  transformation was used to model the surface roughness due to the large variation in roughness values. The surface roughness decreased from 32 μm to 12 μm (effect = 20 μm) when the powder feed rate was increased from 70 g min<sup>-1</sup> to 140 g min<sup>-1</sup>. The surface roughness also decreased from 27 μm to 16 μm (effect = 11 μm) as the substrate temperature was increased from ambient to 87 °C.

Because both parameters are involved in significant interaction effects, it is essential to include such interactions in the empirical model. The surface roughness remained constant at low propane flow rates, even when the substrate temperature increased; however, the roughness decreased with increasing substrate temperatures at the high propane flow rate (effect = 9 μm). The second noteworthy interaction involves stand-off distance and powder feed rate. The surface roughness decreased with increasing powder feed rate at both 25 and 50 cm. At lower feed rates, the roughness is lower for shorter stand-off distances, but at higher powder feed rates, the roughness is lower at longer stand-off distances (effect = 7 μm). The empirical equation used to estimate coating surface roughness (in terms of  $R_a$  in μm) is

$$\ln Y_{\text{roughness}} = 2.81 - 0.49X_{1\text{ coded}} - 0.23X_{1\text{ coded}}X_{2\text{ coded}} - 0.31X_{3\text{ coded}} - 0.21X_{4\text{ coded}} - 0.22X_{3\text{ coded}}X_{4\text{ coded}} \quad (11)$$

Upon analysis of the residuals, this equation is accurate to within 10% of the measured surface roughnesses.

### 3.3. Microstructure: splat elongation ratio

The splat elongation ratio depends on powder feed rate,  $X_1$ , stand-off distance,  $X_2$ , powder feed rate interacting with stand-off distance,  $X_{12}$ , and substrate preheat temperature,  $X_3$ . A number of secondary effects are also included,  $X_{15}$ ,  $X_{25}$ ,  $X_{34}$ , and  $X_{45}$ . The largest effect was observed when the powder feed rate was increased to  $140 \text{ g min}^{-1}$  and thus increased the average elongation ratio from 3.3 to 4.8 (effect = 1.5). The average elongation ratio increased from 3.4 to 4.6 (effect = 1.2) when the stand-off distance was increased from 25 cm to 50 cm. The elongation ratio also increased from 3.6 to 4.4 (effect = 0.8) when the substrate was pre-heated to  $87^\circ\text{C}$ . The powder feed rate was also found to interact with stand-off distance. The splat elongation ratio does not change with stand-off distance at the low powder feed rate,  $70 \text{ g min}^{-1}$ . However, at the higher feed rate corresponding to  $140 \text{ g min}^{-1}$ , the average elongation ratio increased by approximately 2.2 when the stand-off distance increased from 25 cm to 50 cm. The empirical equation used to estimate the splat elongation ratio (non-dimensional units) from knowledge of the chosen process parameters is

$$\begin{aligned}
 Y_{ER} = & 3.99 + 0.75X_{1 \text{ coded}} + 0.59X_{2 \text{ coded}} \\
 & + 0.51X_{1 \text{ coded}}X_{2 \text{ coded}} \\
 & + 0.58X_{1 \text{ coded}}X_{5 \text{ coded}} \\
 & - 0.37X_{2 \text{ coded}}X_{5 \text{ coded}} + 0.41X_{3 \text{ coded}} \\
 & + 0.34X_{3 \text{ coded}}X_{4 \text{ coded}} + 0.35X_{4 \text{ coded}}X_{5 \text{ coded}}
 \end{aligned}
 \tag{12}$$

Again, using the parameters from the experimental matrix and comparing the residuals, this equation was accurate to within 10% of the measured elongation ratio.

### 3.4. Particle velocities

Particle velocities (50 particles per data point) were measured at several stand-off distances for both a high flame setting (high propane, high compressed air) and for a low flame setting (low propane, low compressed air). At a distance of 25 cm from the nozzle, average particle velocities were  $14$  and  $10 \text{ m s}^{-1}$  for the high and low gas settings respectively, Fig. 2. The standard deviation was  $5 \text{ m s}^{-1}$  and indicated that increasing the gas flow rates does not appreciably affect the particle velocity. In addition, particle velocities at 50 cm from the nozzle are only slightly lower than at 25 cm, irrespective of gas settings. Therefore, differences in the measured responses as a function of stand-off distance and gas flow settings cannot be attributed to particle velocity.

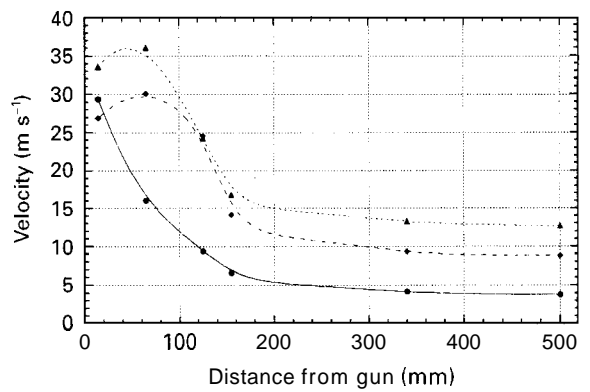


Figure 2 Particle velocities measured at various stand-off distances. (—●—) Powder only, (---◇---) low flame setting, (---△---) high flame setting.

## 4. Discussion

A general trend was observed between the average elongation ratio and surface roughness for each specimen in the matrix. Examining Fig. 3, a greater surface roughness correlates to lower splat elongation ratios and thus poor coalescence. From the DOE study, two factors seem responsible for the poor melt flow characteristics. The first stems from a low thermal input to the polymer via a short residence time within the flame. This results in insufficient particle melting and thus low elongation ratios. On the coating surface, low splat elongation ratios correspond to an agglomeration of fused polymer spheres. Areas of protruding polymer particulates yield a higher surface roughness and define a poorly coalesced coating. The second possibility relates to the rate of polymer injection into the combustion zone. A low powder feed rate equates to a lower deposited polymer per unit area. Less molten material can conform to the underlying topography. Discontinuous surface coverage will result in a higher surface roughness unless a slower traverse speed is chosen.

The temperature dependence upon surface roughness is shown in Fig. 4. A high surface roughness was measured for coating temperatures lower than  $80^\circ\text{C}$ . The surface roughness decreased by a factor of  $\approx 2$  at temperatures greater than  $90^\circ\text{C}$ . This transition is in agreement with the melting point of the copolymer

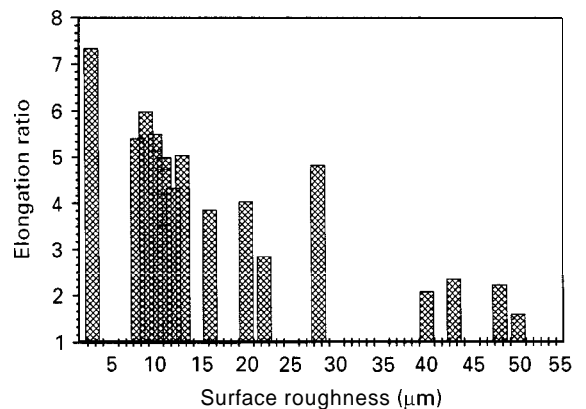


Figure 3 Relationship between splat elongation ratio and surface roughness.

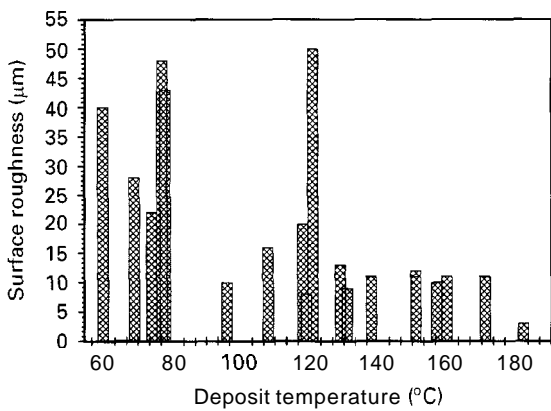


Figure 4 Relationship between surface roughness and deposit temperature.

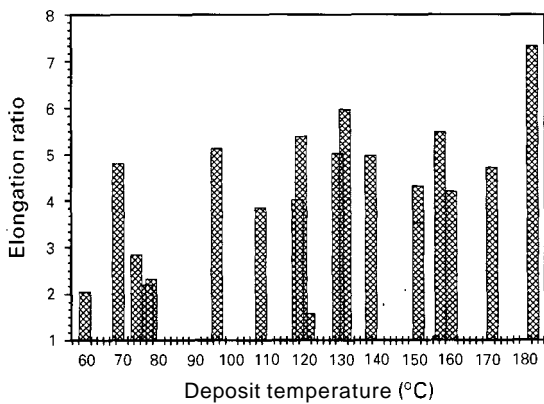


Figure 5 Relationship between elongation ratio and deposit temperature.

which occurs at approximately 90°C. However, the elongation ratio measurements, Fig. 5, were not as sensitive to temperature as the surface roughness measurements. The elongation ratio only correlated to the coating temperature at the extreme temperature limits. The temperature region of 95–140 °C may be sufficient to reduce the surface roughness, but temperatures within this range are not sufficiently high to elongate the polymer splats. At 180 °C, a noticeable increase in splat elongation ratio occurred. Differences in elongation ratio did not arise from differences in particle velocities because the velocities were found to be independent of the gas flow rates and stand-off distance. It also should be noted that the splat elongation ratio is a function of the original diameter of the polymer particulate. Larger polymer particles will remain more spherical in shape than smaller particles. Less energy is required to melt the fine particles, thus smaller sized particles are more susceptible to deformation at the site of impact than the larger polymer particulates.

Differences in the melting and/or deformation behaviour of EMAA copolymer can be discerned by examining the microstructures in cross-section. Fig. 6 illustrates poor coating coalescence due to insufficient polymer melt-flow as evident by spherical splats (specimen 7, Table II). The degree of melting and coalescence in Fig. 7 (specimen 16, Table II) is higher as

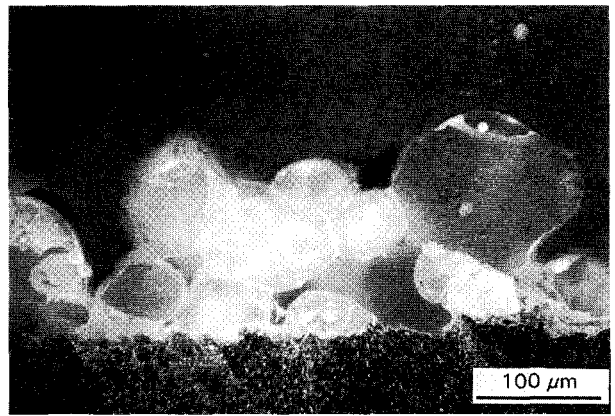


Figure 6 Poor coalescence exhibited by low elongation ratios.

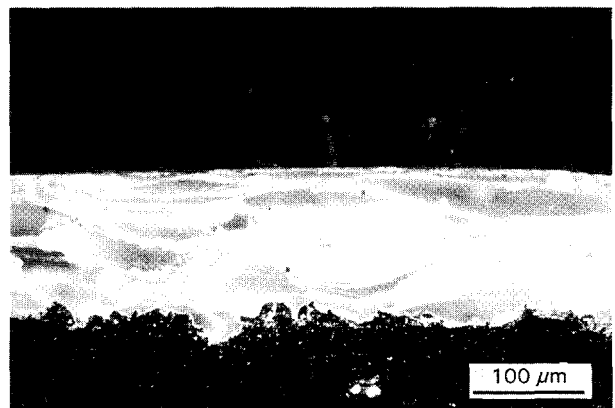


Figure 7 High coalescence exhibited by high elongation ratios

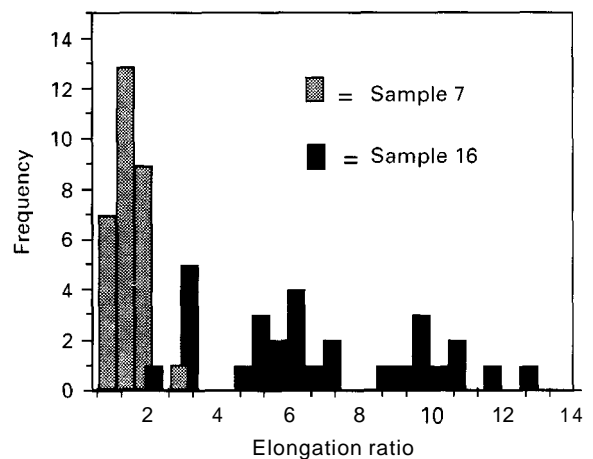


Figure 8 Distribution of splat elongation ratios for the microstructural extremes.

evident by thin lamellae and a deformed impact geometry. The impinging molten polymer will flow around the underlying topography, thereby increasing the density of splats.

The elongation ratio distributions for the poorly coalesced coating and highly coalesced coating are shown in Fig. 8. The average elongation ratio for the microstructure in Fig. 6 was 1.6 with a standard deviation of 0.4. 90% of the coating contains particles with

elongation ratio less than 2. In contrast, the average elongation ratio for the coating in Fig. 7 was 7.3 with a standard deviation of 3.6. This coating, which corresponds to the lowest of the measured surface roughness values, reveals that less than 2% of the deposit contains particles with elongation ratios lower than 2. Although it is common for poorly melted particles to exist in the coating due to the different particle trajectories through the flame, such an analysis quantifies the microstructural variation in thermal-sprayed EMAA coatings.

Properties of polymer coatings depend on the molecular weight of the average polymer chain. A higher molecular weight polymer, hence a polymer of lower melt flow index, will impart greater toughness and temperature resistance. The longer the polymer chain, the greater the number of entanglements, hence more energy is necessary to disentangle the molecules. However, higher molecular weight ( $M$ ) chains have lower self-diffusion coefficients, scaling as  $M^{-2}$  according to reptation theory [15]. A lower molecular weight polymer is therefore used for situations requiring lower deposition temperatures. Ethylene-methacrylic acid copolymer coatings with respective melt flow indices of 500 (PF113) and 32 (PF111) were sprayed using the same spray parameters (sample 17, Table II). The lower molecular weight formulation received sufficient energy to melt the particulates, as is evident by the elongated lamellae, Fig. 9. The higher molecular weight polymer particles did not receive enough thermal energy and spherical-like splats arose, Fig. 10.

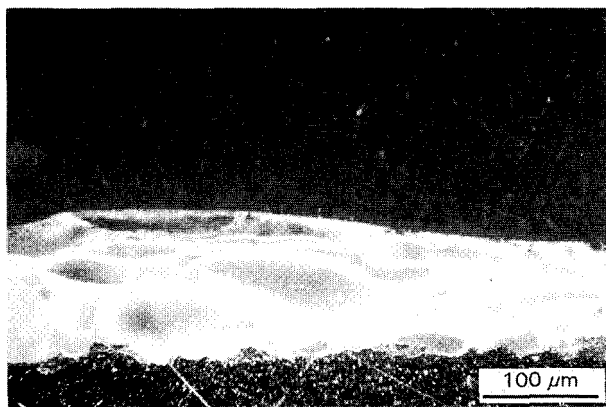


Figure 9 Cross-section of PF113

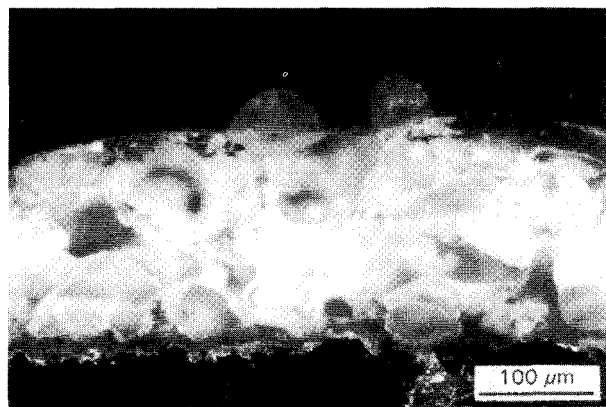


Figure 10 Cross-section of PF111.

Thus, polymer molecular weight significantly affects the morphology of the solidifying particles. A higher heat transfer from the flame to the particle is necessary to induce greater particulate spreading for higher molecular weight EMAA formulations. This can be accomplished by either increasing the particle residence time within the flame or using a slower traverse speed.

## 5. Conclusion

The microstructure of a combustion-sprayed polymer deposit is process controlled. A design of experiments approach was used to study the melting and coalescence of a low molecular weight EMAA copolymer. The substrate preheat temperature showed the largest effect on coating temperature. An empirical equation was developed to estimate coating temperature to within 5% error. The powder injection rate showed the largest effect on coating surface roughness and splat elongation ratio. Polynomial equations were also experimentally determined for surface roughness and splat elongation ratio to be accurate within 10%.

Centreline particle velocities did not change with the gas flow rates or stand-off distances used in this study ( $\sim 15 \text{ m s}^{-1}$ ); however, differences in the splat elongation ratio were observed. The particle residence time varied from 3 ms for a 5 cm length flame to 13 ms for a 20 cm length flame. The flame stoichiometry did not appreciably affect the fusion of the polymer particulates, thus, for a fixed traverse speed, the particle residence time within the flame as well as the number of particles arriving at the substrate surface determines the extent of EMAA coating coalescence.

Examining the correlations between the responses, a well-coalesced EMAA coating (melt flow index of 500 g/10 min) will have a temperature greater than  $125^\circ\text{C}$ , a surface roughness less than  $15 \mu\text{m}$ , and a splat elongation ratio of at least 4.5. The coating temperature, surface roughness and microstructure can be estimated on the basis of the selected process parameters.

## Acknowledgements

The authors thank Plastic FlameCoat Systems for the use of the spray torch and ethylene-methacrylic acid copolymer powder, William Smith for conducting particle velocity measurements, the US Army Corps of Engineers, and NSF MSS9311053.

## References

1. T. RACE, V. HOCK and A. BEITELMAN, J. *Protect. Coat. Linings* **6**(1) (1989) 37.
2. T. KATAUSKAS, *Res. Devel.* May (1990) 42.
3. J. A. APOSTOLOS, D. M. PARKS and R. A. CARELLO, *Mater. Perform.* **26**(12) (1987) 22.
4. R. H. UNGER, "Thermal Spray: Advances in Coating Technology, edited by D. Houck (ASM, Materials Park, OH, 1988) pp. 399-406.
5. J. A. BROGAN, J. MARGOLIES, S. DROZDZ, S. SAMPATH, H. HERMAN and C. C. BERNDT, in "1995 Advances in Thermal Spray Science and Technology", edited by S. Sampath and C. C. Berndt (ASM, Materials Park, OH, 1995) pp. 521-26.

6. G. K. SWEET. in "Thermal Spray Coatings: Research Design and Applications", edited by C. C. Berndt and T. F. Bernecki, (ASM, Materials Park, OH, 1993) pp. 381-84.
7. Y. BAO and D. T. GAWNE, *ibid.* pp. 417-22.
8. P. J. LOUSTAUNAU and D. HORTON, *Mater. Perform.* **33**(7) (1994) 32.
9. T. W. GLASS and J. A. dePAY. "Thermal Spray Coatings: Properties, Processes and Applications", edited by T. F. Bernecki (ASM, Materials Park, OH, 1991) pp. 345-51.
10. A. ROGERSON, *J. Protect. Coat. Linings* **11**(8) (1994) 25.
11. J. REIMER, US Pat. 4632309, 30 December 1986, 11pp.
12. J. A. BARNARD and J. N. BRADLEY, "Flame and Combustion", (Chapman and Hall, New York, 1985).
13. E. P. BOX, W. G. HUNTER and J. S. HUNTER, "Statistics for Experimenters", (Wiley, New York, 1978).
14. J. AGAPAKIS and T. HOFFMAN, *JTST* **1**(1) (1992) 19.
15. P. G. de GENNES, *J. Chem. Phys.* **55** (1971) 572.

*Received 8 January  
and accepted 18 March 1996*